

# Variability and stellar populations with deep optical-IR images of the Milky Way disc: matching VVV with VLT/VIMOS data<sup>★,★★</sup>

P. Pietrukowicz<sup>1</sup>, D. Minniti<sup>2,3</sup>, J. Alonso-García<sup>2</sup>, and M. Hempel<sup>2</sup>

<sup>1</sup> Warsaw University Observatory, Al. Ujazdowskie 4, 00-478 Warszawa, Poland  
e-mail: pietruk@astrouw.edu.pl

<sup>2</sup> Departamento de Astronomía y Astrofísica, Pontificia Universidad Católica de Chile, Av. Vicuña MacKenna 4860, Casilla 306, Santiago 22, Chile

<sup>3</sup> Vatican Observatory, Vatican City State V-00120, Italy

Received -; accepted -

## ABSTRACT

**Aims.** We have used deep  $V$ -band and  $JHK_s$ -band observations to investigate variability and stellar populations near the Galactic plane in Centaurus, and compared the observations with the Galactic model of Besançon.

**Methods.** By applying image subtraction technique to a series of over 580  $V$ -band frames taken with the ESO VLT/VIMOS instrument during two contiguous nights in April 2005, we have detected 333 variables among 84 734 stars in the brightness range  $12.7 < V < 26.0$  mag. Infrared data collected in March 2010 with the new ESO VISTA telescope allowed us to construct deep combined optical-IR colour-magnitude and colour-colour diagrams.

**Results.** All detected variables but four transit candidates are reported for the first time. The majority of the variables are eclipsing/ellipsoidal binaries and  $\delta$  Scuti-type pulsators. The occurrence rate of eclipsing/ellipsoidal variables reached  $\sim 0.28\%$  of all stars. This is very close to the highest fraction of binary systems detected using ground-based data so far (0.30%), but still about four times less than the average occurrence rate recently obtained from the *Kepler* space mission after 44 days of operation. Comparison of the observed  $K_s$  vs.  $V - K_s$  diagram with a diagram based on the Besançon model shows significant effects of both distance and reddening in the investigated direction of the sky. We demonstrate that the best model indicates the presence of absorbing clouds at distances 11-13 kpc from the Sun in the minor Carina-Sagittarius Arm.

**Key words.** Stars: variables: general – variables: delta Scuti – binaries: eclipsing – Galaxy: disc – Galaxy: structure – Hertzsprung-Russell and C-M diagrams

## 1. Introduction

In recent years our knowledge on the structure of the Milky Way Galaxy has greatly improved thanks to wide-field photometric surveys conducted from ground-based and orbital telescopes. They are usually dedicated to the detection of particular objects, such as transiting extrasolar planets, microlensing events, or gamma ray burst afterglows, e.g., MACHO (Alcock et al. 2000), OGLE (Udalski et al. 2003), HAT (Bakos et al. 2004), ROTSE (Woźniak 2004), ASAS (Pojmański 2001), and the *Kepler* space mission (Koch et al. 2010). However, these surveys also discover an enormous amount of new variable objects of different types (e.g., Woźniak et al. 2002; Pojmański et al. 2005; Nataf et al. 2010). Variable stars provide important information about the structure and evolution of stars as well as the whole Galaxy (e.g., Alcock et al. 1998; Szczygieł et al. 2009).

The most recent view of the Galactic plane regions has been presented by Churchwell et al. (2009) based on the *Spitzer*/GLIMPSE surveys. The large-scale structure of the Galaxy has been traced by red-clump giants to reveal the ra-

dius and orientation of the central bar, thanks to characteristic changes in star counts for  $|l| < 65^\circ$  as a function of Galactic longitude at a wavelength of  $4.5 \mu\text{m}$ .

A useful method to investigate structure and stellar populations in the Galaxy is the comparison of synthetic magnitude histograms, colour-magnitude diagrams (CMDs), and colour-colour diagrams with real data (Lucas et al. 2008). Here, we construct deep (down to  $V \approx 26.0$  mag and  $K_s \approx 18.6$  mag) optical-IR colour-colour and colour-magnitude diagrams of two southern Galactic plane fields. For one of these fields we present the results of a search for variable stars and compare the observed  $K_s$  vs.  $V - K_s$  diagram with a theoretical one based on the Galactic model of Besançon (Robin et al. 2003). Our results show the great potential of ongoing and upcoming large visual and near-infrared surveys, such as LSST (Large Synoptic Survey Telescope, Ivezić et al. 2008), VVV (Vista Variables in Via Lactea, Minniti et al. 2010), or Pan-STARRS (Kaiser et al. 2002).

## 2. Observations and data reduction

The observations presented in this work were carried out with the ESO VISTA and UT3 telescope at Paranal Observatory. The infrared observations were collected with the new 4.1-m Visible and Infrared Survey Telescope for Astronomy (VISTA) as a part of the VISTA Variables in the Via Lactea (VVV) ESO Public Survey (Minniti et al. 2010). The telescope is equipped with a

\* Based on observations collected with the VLT and VISTA telescopes at Paranal Observatory (ESO Programmes 075.C-0427(A) and 179.B-2002(B), respectively)

\*\* Photometry and data table on detected variables are available in electronic form at the CDS via anonymous ftp to cdsarc.u-strasbg.fr (130.79.128.5) or via http://cdsweb.u-strasbg.fr/cgi-bin/qcat?J/A+A/000/000

$16 \times 2048 \times 2048$  pixel near-IR camera with a pixel size of  $0''.34$ . The monitored area of the VVV survey covers the Galactic bulge ( $-10^\circ < l < +10.5^\circ$ ,  $-10^\circ < b < +5.6^\circ$ ) and an adjacent section of the Galactic plane ( $-65^\circ < l < -10^\circ$ ,  $-2.25^\circ < b < +2.25^\circ$ ). Planned observations span the years 2010-2014 with the main variability monitoring campaigns in 2012 (bulge area) and 2013 (disc area). We used the DOPHOT package (Schechter et al. 1993) to extract photometry from images obtained with VISTA.

Optical data were obtained with VIMOS at the 8.2-m Unit Telescope 3 (UT3) of the Very Large Telescope in April 2005. VIMOS is an imager and multi-object spectrograph (LeFevre et al. 2003). Its field of view consists of four quadrants of about  $7' \times 8'$  each, separated by a cross,  $2'$  wide. Each CCD has  $2048 \times 2440$  pixels with a pixel size of  $0''.205$ . The main goal of that programme was to perform a photometric follow-up of over 30 OGLE transiting candidates spread over four VIMOS fields in the constellations Carina, Centaurus and Musca. Some individual results were published by Fernández et al. (2006), Díaz et al. (2007), Hoyer et al. (2007), Minniti et al. (2007), Pietrukowicz et al. (2009) and Pietrukowicz et al. (2010).

The work presented here focuses on two VIMOS fields located within the VVV area in Centaurus. They contain OGLE-TR-167 and OGLE-TR-170, both classified as planetary transit candidates by Udalski et al. (2004), but currently known as eclipsing systems (Pietrukowicz et al. 2010). We will refer to the fields as F167 and F170, respectively. They are located within the VVV tiles<sup>1</sup> d009 and d008, respectively. The field F167 was monitored for two hours in the night of 2005 April 9, and during the whole night of 2005 April 10, while the field F170 was observed for the whole two subsequent nights of 2005 April 11-12. All VIMOS images were taken in the V-band only. Three hundred ninety-five and 583 exposures were obtained in the fields F167 and F170, respectively. Table 1 gives basic information on these fields.

The periphery of each VIMOS quadrant suffers from coma. Therefore, we reduced the field of view to  $1900 \times 2100$  pixels, which then covered  $7'.18 \times 6'.49$ . The total field in which we searched for variable objects equals  $186.3 \text{ arcmin}^2$ . In Fig. 1 we show the location of the two VIMOS fields overlaid on a part of the VVV disc area.

Owing to the longer time span and larger number of images taken in the field F170, we decided to focus our search in this field. The photometry was extracted with the help of the *Difference Image Analysis Package* (DIAPL) written by Woźniak (2000) and modified by W. Pych<sup>2</sup>. The package is an implementation of a method developed by Alard & Lupton (1998). To obtain higher quality photometry, we divided the field into  $475 \times 525$  pixel subfields.

Reference frames were constructed by combining nine of the highest quality individual images, i.e. with the best seeing and low background. The profile photometry for the reference frame was extracted with DAOPHOT/ALLSTAR (Stetson 1987). These measurements were used to transform the light curves from differential flux units into instrumental magnitudes, which were subsequently transformed into standard V-band magnitudes by adding an offset derived from V-band magnitudes of the planetary transits located in the field. The quality of the photometry is illustrated in Fig. 2.

<sup>1</sup> For the definition of the tile see the VVV description paper by Minniti et al. (2010)

<sup>2</sup> The package is available at <http://users.camk.edu.pl/pych/DIAPL/>

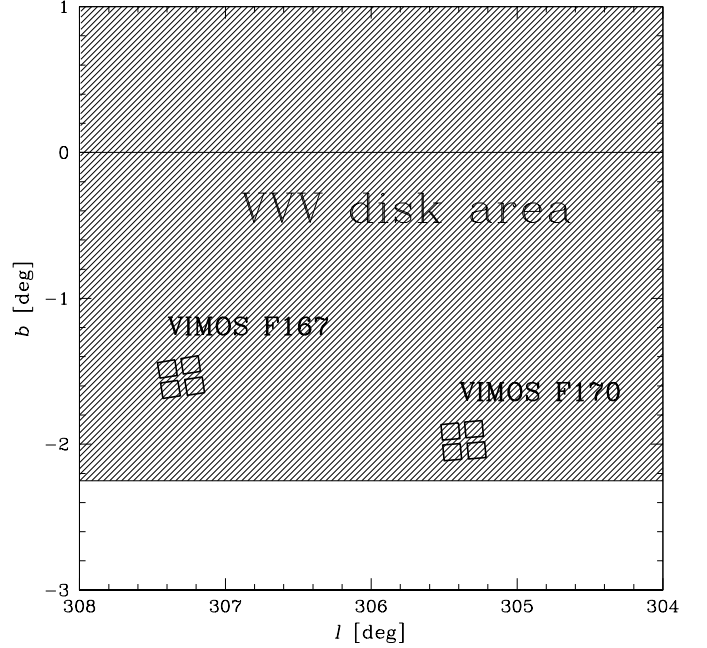


**Fig. 1.** Location of the analysed fields in Galactic coordinates.

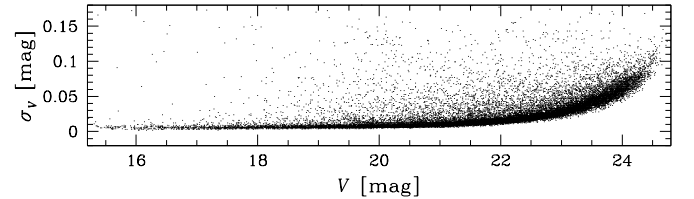


**Fig. 2.** Photometric errors for 22 717 stars detected in the VIMOS quadrant A2 of the field F170 plotted as a function of V-band magnitude.

### 3. The variables

Owing to the relatively short period of the VIMOS observations in the field F170 (only two contiguous nights), we decided to look for variables only by direct eye inspection of all 84 734 extracted light curves. The total number of detected variables reached 333 objects. All objects, except OGLE-TR-170, OGLE-TR-171 (Udalski et al. 2004), and transit-3 and transit-4 (Pietrukowicz et al. 2010) are new identifications. We used no automatic methods for the search. Previous experience with the four-night data in the VIMOS field F113 towards the constellation Carina (Pietrukowicz et al. 2009) showed us that about one third of the periodic variables were missed in the automatic search and merely four additional objects were found in comparison to the simple eye inspection. For the two-night data in Centaurus this would be even less effective.

All detected variables were sorted by increasing right ascension and classified by considering the shape of the light curves and possible periodicity. In Table 2 we provide a census of the different types of variables found in field F170. It is worth to compare this table with Table 2 in Pietrukowicz et al. (2009), which was prepared for the field F113, located at similar galactic latitude but  $\sim 16^\circ$  farther away from the Galactic centre. The lower percentage of detected variables, 0.393% vs. 0.692%, can

**Table 1.** Characteristics of the observed fields. Coordinates are given for the centres of the fields. Reddening values were taken from Schlegel et al. (1998).

VIMOS field	VVV field	RA(2000.0) [h:m:s]	Dec(2000.0) [°:′:″]	$l$ [°]	$b$ [°]	$E(B - V)$ [mag]
F167	d009	13:31:36.00	-64:04:15.0	307.306	-1.541	1.7 - 2.1
F170	d008	13:14:17.60	-64:44:21.0	305.368	-1.976	1.0 - 1.4

be explained by the shorter time coverage of the observations (two nights vs. four nights). An interesting result is the very similar percentage of eclipsing/ellipsoidal variables in both samples: 0.284% in F170 vs. 0.291% in F113. We were able to confirm the periodic nature of 263 stars out of 329 newly discovered variables. We derived the periods of 210 out of 237 new eclipsing/ellipsoidal binary systems. The incident rate of observed  $\delta$  Scuti-type pulsators in field F170 is about three times lower than in field F113. The detection of this type of low-amplitude variables strongly depends on their distance. The majority of the stars in field F170 are objects located in the Scutum-Centaurus Arm, while most of the stars observed in field F113 are likely located closer to us in the minor Carina-Sagittarius Arm.

In Figs. 3 to 6 we present some example light curves of the variables found in the VIMOS field F170. The eclipsing binaries V004, V042, and V247 in Fig. 3 are among the faintest variables in the sample. The detection of a flare in the light curve of star V014 is one of the more peculiar results. Similarly we note the rising part in the light curve of the eclipsing object V159 in Fig. 4. Close inspection showed that it is an isolated star located far from any edges and defects of the VIMOS chip. Most of the long-time scale variables illustrated in Fig. 6 exhibit monotonic changes in brightness. Object V081 presents an interesting light curve with a flat curve in the first night followed by a smooth up and down 0.04 mag amplitude variation on the second night. Additional photometry would help to classify these objects and to estimate the periods more accurately.

All photometric data presented in this paper, finding charts, and a large table with coordinates, periods, and magnitudes of the detected variables are available via anonymous ftp to ftp.astrouw.edu.pl/pub/pietruk/VIMOSvar/ or cdsarc.u-strasbg.fr.

#### 4. Matching optical and infrared data

We have matched the  $V$ -band data obtained with VIMOS for the fields F167 and F170 with  $JHK_s$ -band observations from VISTA using equatorial coordinates. Prior to this operation we prepared

**Table 2.** Census of variables detected in the VIMOS field F170.

Type of stars	Number	Percentage
All stars searched for variability	84734	100 %
All variables	333	0.393 %
All binaries	241	0.284 %
Eclipsing/ellipsoidal with known period	210	
Transiting	4	
Other eclipsing	27	
Pulsating variables	53	0.063 %
$\delta$ Scuti	47	0.055 %
Other pulsating	6	
Long-time scale variables	38	0.045 %
Stars with flares	2	0.002 %

auxiliary maps showing positions of stars from both lists and we applied position corrections in each VIMOS quadrant. Because of the large difference in brightness of stars in the optical and infrared passbands and the effect of coma in the corners of the VIMOS detectors we decided to set a matching radius of  $1''.2$ , and to reject all ambiguous objects from the final list.

#### 4.1. Star count histograms

Table 3 gives numbers of all detected and matched stars together with magnitude range in the  $V$  and  $K_s$  bands. The difference of 0.8 mag in the  $K_s$ -band limit for the brightest stars between the two fields results from different saturation values of chips of the infrared camera at the VISTA telescope.

**Table 3.** Census and magnitude range of all analysed stars in fields F167 and F170.

Field (VIMOS-VVV)	F167-d009	F170-d008
All stars detected in the $V$ band	89694	84734
All stars detected in the $K_s$ band	43852	62460
Common stars	28710	42813
$V$ -band range [mag]	12.5-25.9	12.7-26.0
$K_s$ -band range [mag]	13.2-18.6	12.4-18.6

Figs. 7 and 8 illustrate the star count histograms for fields F167 and F170, respectively. The histograms clearly show that the number of stars in the  $K_s$ -band increases more rapidly than the one in the  $V$ -band. From the location of maxima in the  $V$ -band (upper panels) one can find that the optical data from VIMOS are about 1 mag deeper than the near-IR data from VISTA. In the lower panel of Fig. 8 we add a profile based on the Besançon Galactic model, which we describe in detail in Sec. 6. From the comparison of the models with the observations we can infer that the analysed data are complete down to  $K_s \sim 17.5$  mag.

#### 4.2. Colour-magnitude and colour-colour diagrams

In Fig. 9 we show  $K_s$  vs.  $V - K_s$  CMDs for the two observed VIMOS fields. The main features in both diagrams are the main sequence and the area of red giants. This is particularly obvious in field F170, where the saturation level is higher. Significant distance and reddening effects can be easily noted. The red giants spreads over at least 2 mag in the  $K_s$ -band ( $12.5 < K_s < 14.5$  mag) and 1 mag in colour ( $4.5 < V - K_s < 5.5$  mag). According to the newest view of our Galaxy (Churchwell et al. 2009), most observed stars in these two fields are very likely objects located in the Scutum-Centaurus Arm, which is tangent to the line of sight in this direction. Distances of these stars are very likely in the range from 4 to 10 kpc. Assuming a maximum reddening of  $E(B - V) \sim 2.1$  mag in the investigated disc fields (Schlegel et al. 1998), and a 'universal' extinction

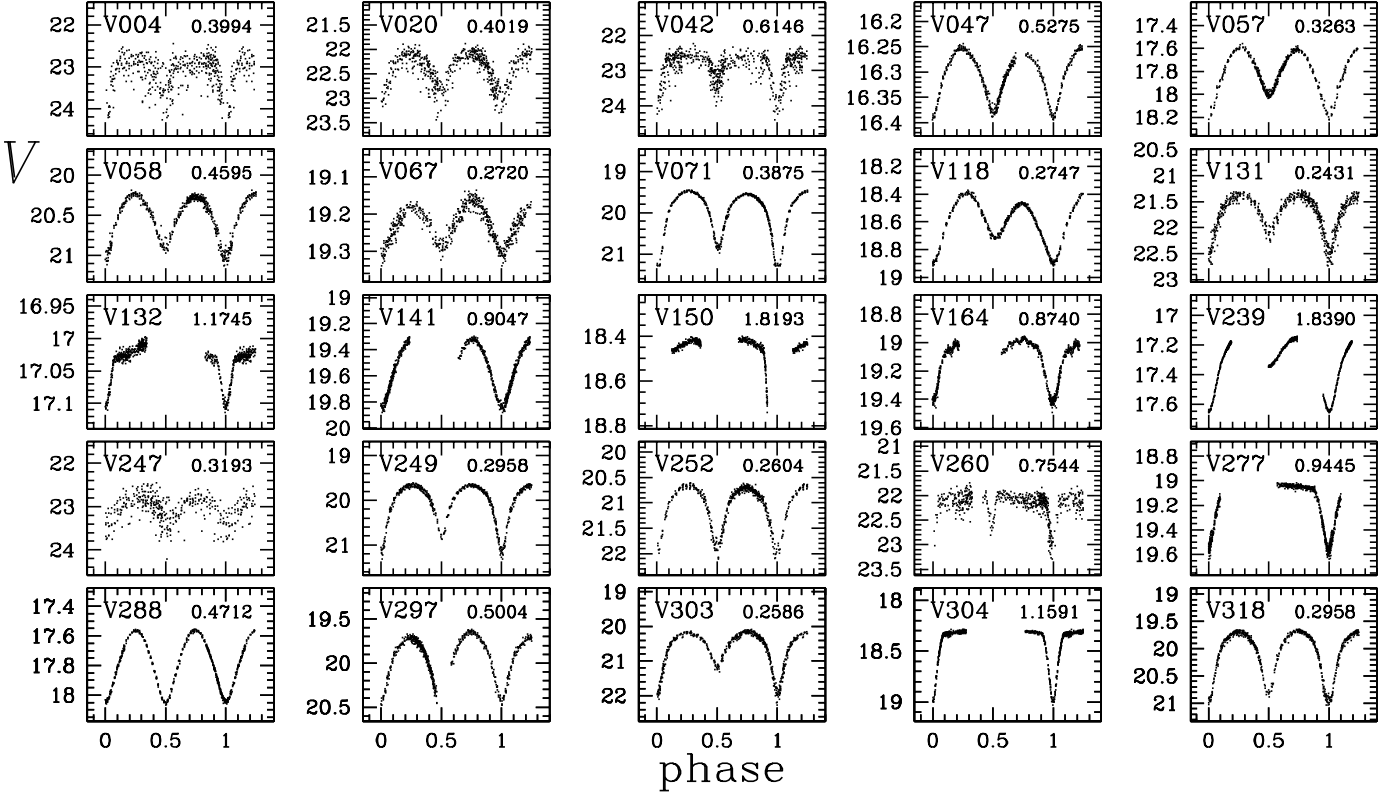


**Fig. 3.** Examples of phased light curves of eclipsing/ellipsoidal variables with estimated period (in days). Note that in object V014 we observed a flare of an amplitude of 0.1 mag.

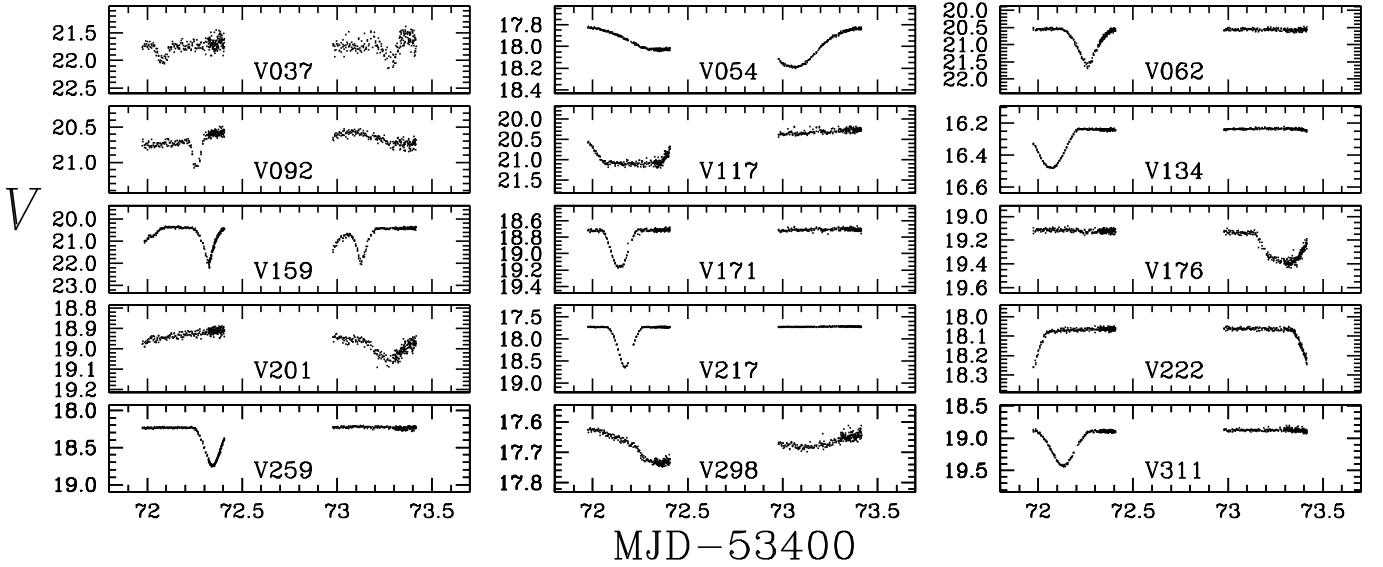


**Fig. 4.** Examples of light curves of eclipsing variables with unknown period.

law  $A_V = 3.1E(B - V)$ , we obtain a maximum absorption of  $A_V \sim 6.5$  mag.

Fig. 9 also shows a lack of faint clump giants (with  $K < 15$  mag), which can be interpreted as the line of sight leaving the stellar edge of the Milky Way plane (Minniti et al. 2011).

For the two VIMOS fields we have also constructed Hess diagrams using a bin size of 0.2 mag in  $K_s$  and 0.4 mag in  $V - K_s$ , and shown in Fig. 10 together with the subtraction of the

F167 diagram from that of F170. The results confirm that the reddening in field F167 is higher than in F170, as it is to be expected because of its slightly closer position to the Galactic plane ( $b_{F170} \approx -2.0^\circ$  vs.  $b_{F167} \approx -1.5^\circ$ ).

Fig. 11 shows  $J$  vs.  $J - K_s$  CMDs for the two VIMOS fields. Here we arbitrarily separated red giants from main sequence stars with a solid line. The two luminosity classes are also marked in the colour-colour diagrams presented in Fig. 12.

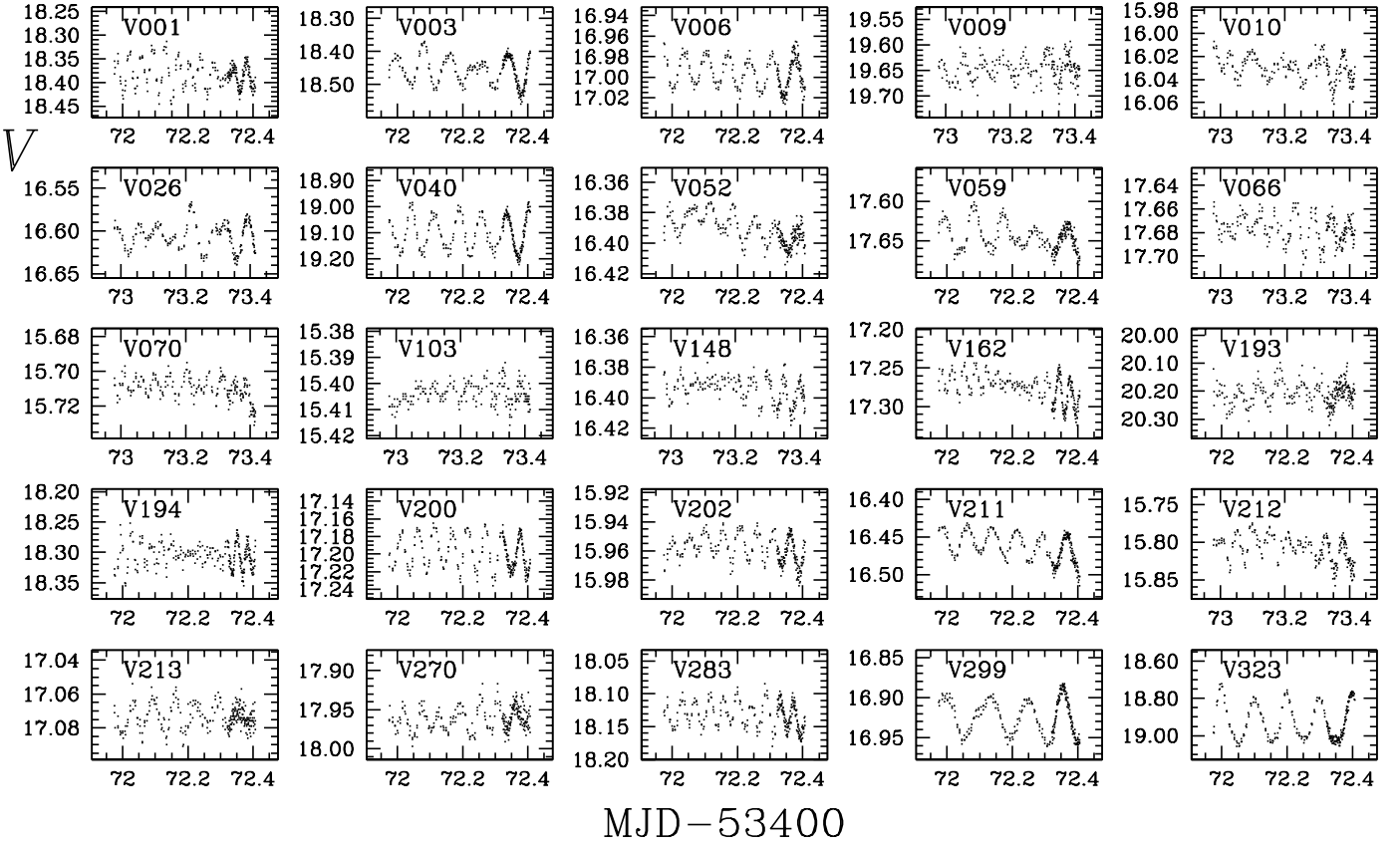


Fig. 5. Examples of light curves of detected  $\delta$  Scuti-type variables. Each panel presents data points from a single night only.

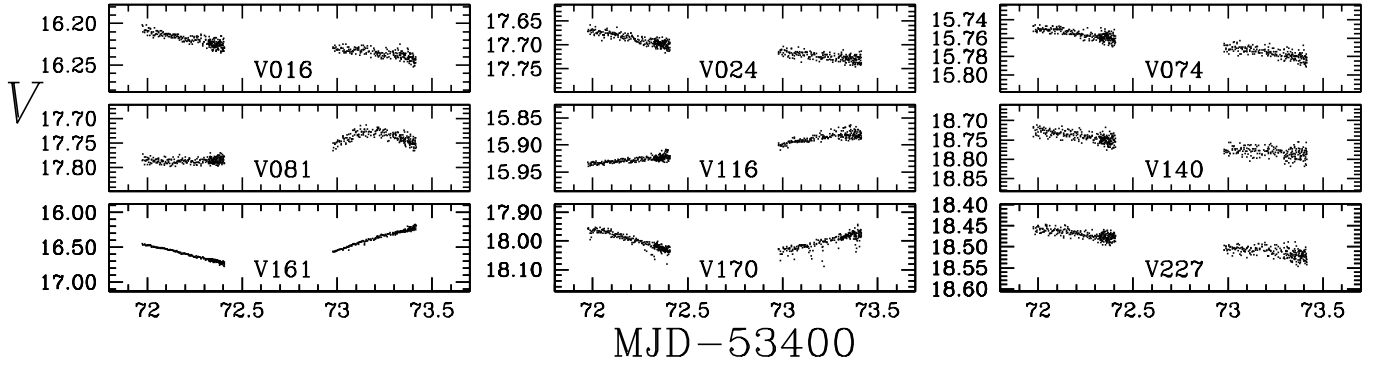


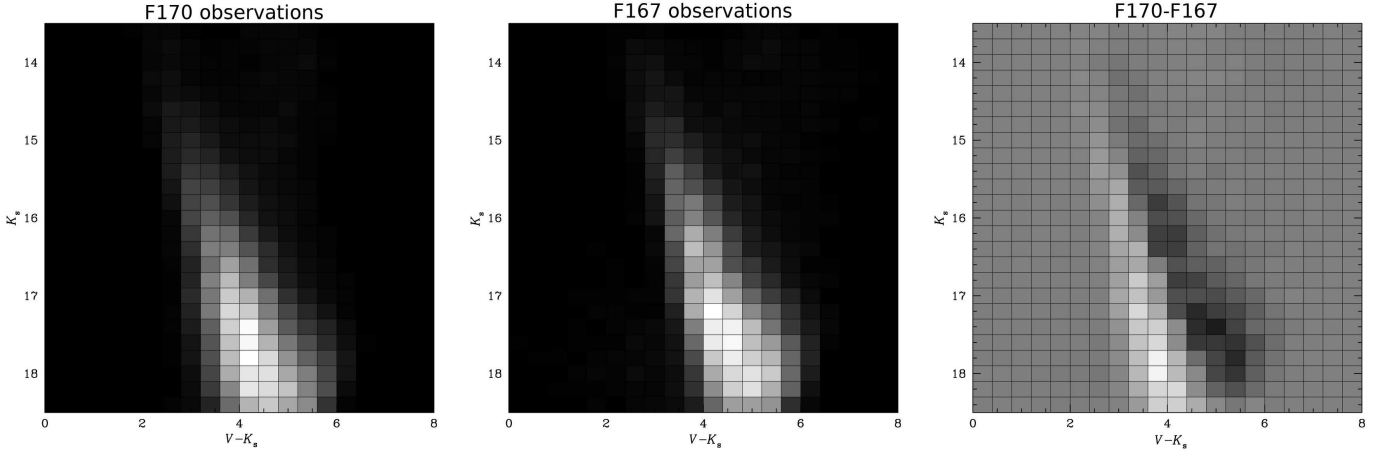
Fig. 6. Light curves of miscellaneous variables of long-time scale brightness changes.

Of the 333 detected variables in field F170 we have obtained  $K_s$ -band magnitudes for 223 with VISTA. We marked the positions of these objects in the  $K_s$  vs.  $V - K_s$  diagram presented in Fig. 13. We stress that their positions in the CMD are still uncertain, because  $K_s$ -band light curves and consequently average magnitudes are not available yet. At this point we are able to infer the following: (1) probably all observed eclipsing and ellipsoidal variables are main-sequence binaries; (2) four transiting objects are main-sequence stars; (3) most of the detected  $\delta$ -Scuti pulsators seem to be located in the closer part of the Scutum-Centaurus Arm. The last point results from the fact that  $\delta$ -Scuti variables have low amplitudes of 0.01 – 0.12 mag. This type of stars placed in the arm should have  $13 < V < 24$  mag (assuming

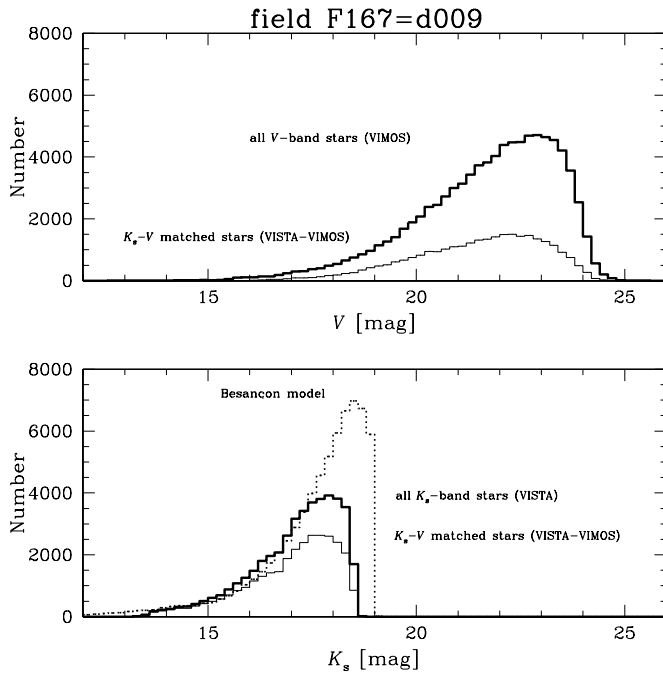
$A_V < 6.5$  mag), whereas we have detected  $\delta$ -Scuti pulsators with  $15.7 < V < 19.6$  mag.

## 5. Comparison with the Galactic model of Besançon

We have compared our data with the stellar population synthesis model of our Galaxy developed by the Besançon group (Robin et al. 2003). For the purpose of this work we have simulated a model assuming a total integration time of 10 Gyr, constant star-formation rate, and no kinematic effects. This was done for stars of absolute brightness  $-7 < M_V < +20$  mag, spectral types between O0 and D5, luminosity classes I to VI, and distances up to 50 kpc from the Galactic center. The selected



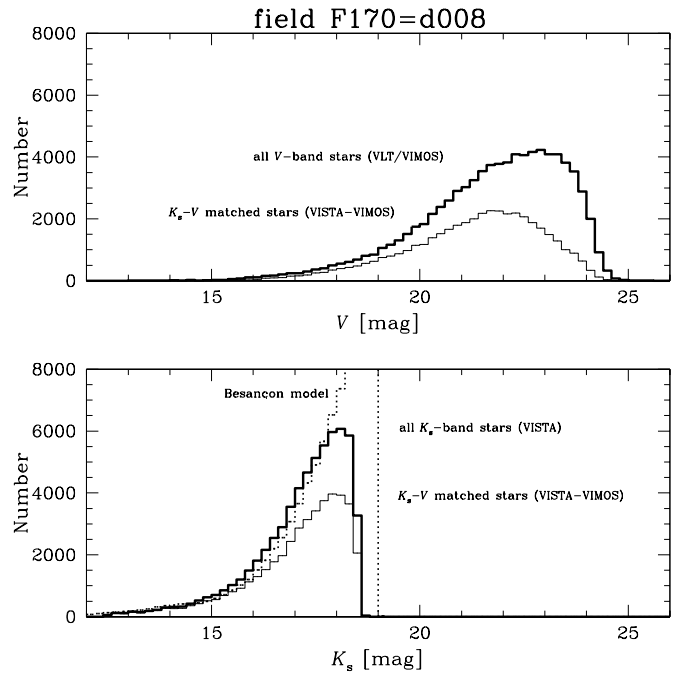
**Fig. 10.** Hess  $K_s$  vs.  $V - K_s$  diagram for the field F170 (left panel) and F167 (middle panel). The subtraction of these two diagrams is shown in the right panel.



**Fig. 7.** Star count histograms in the  $V$ - (upper panel) and  $K_s$ -bands (lower panel). The thin-line profiles show common VIMOS-VVV stars. The Besançon Galactic model is represented by the dotted line. Note that around  $K_s = 17.5$  mag the model departs from the real data.

sky region in our study includes the thin disc, thick disc, and the spheroidal halo. In the Besançon model the disc truncates at 14.0 kpc from the Galactic centre located at a distance of 8.5 kpc from the Sun. The profile densities of stars and interstellar matter are described by the Einasto law. We have tested models with different values of diffuse extinction  $a_V$  and additional discrete clouds of a given absorption  $A_V$ . The model output is a list of synthetic stars with information on distance, absolute magnitude, luminosity class, age, mass, metallicity, and observed magnitudes and colours.

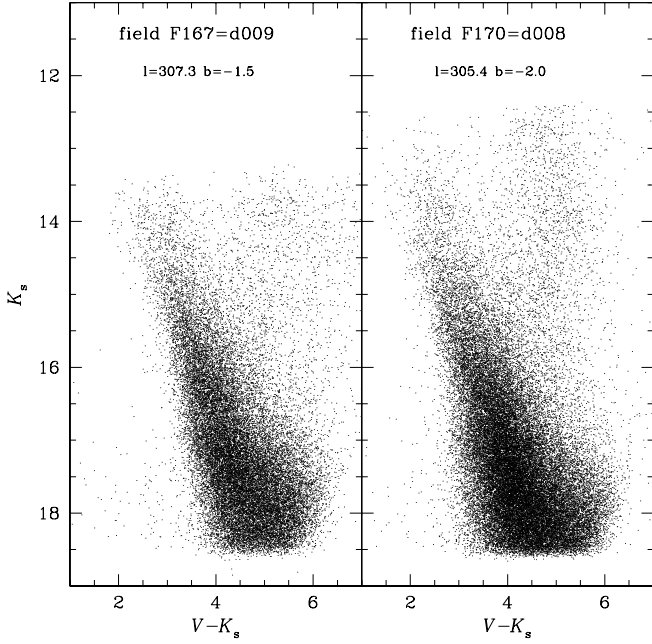
In Fig. 14 we compare two modelled  $K_s$  vs.  $V - K_s$  diagrams with the observed one for field F170. The colours in the syn-



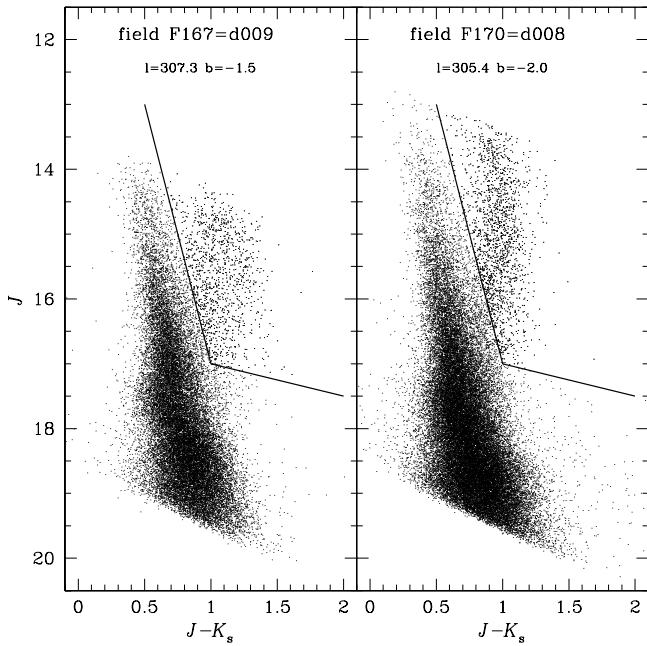
**Fig. 8.** Same as in Fig. 7 but for field F170.

thetic CMDs represent different luminosity classes. The first of the modelled diagrams (in the middle panel) is for the standard value of extinction  $a_V = 0.70$  mag/kpc and without clouds. In general the observations and this model agree well, indicating that the model is not missing any important components. For example, based on the model, we can recognize subgiant stars in the observed CMD around  $K_s \sim 15.5$  mag and  $V - K_s \sim 4.0$  mag.

There are also differences between the first model and observations. The most noticeable difference is the spread in the  $V - K_s$  colour for giants, which is much wider in the observational diagram. This effect partially stems from significant differential reddening in the observed field, but can also be improved by adding interstellar clouds. One can also see too many simulated stars within the area between  $16.0 < K_s < 17.8$  mag and  $2.2 < V - K_s < 2.8$  mag (see boxed section in all panels of Fig. 14), which are actually not observed. In the first mod-

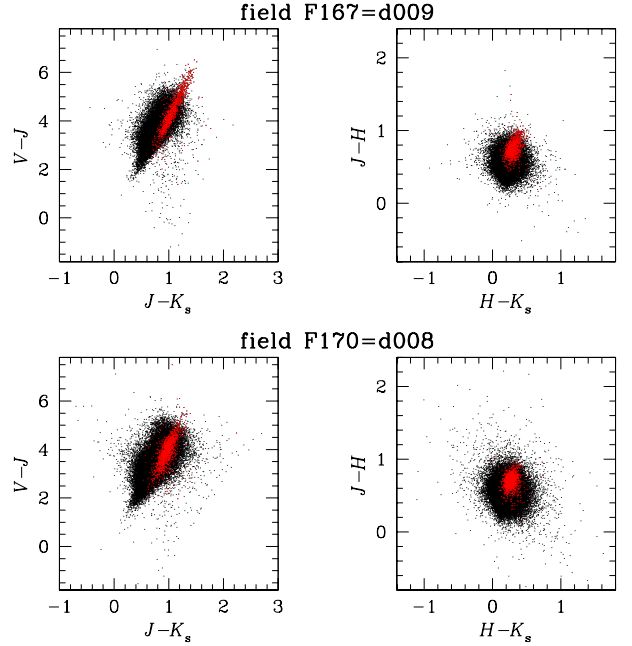


**Fig. 9.**  $K_s$  vs.  $V - K_s$  diagrams for common VIMOS-VVV stars in the VIMOS fields F167 (left panel) and F170 (right panel).

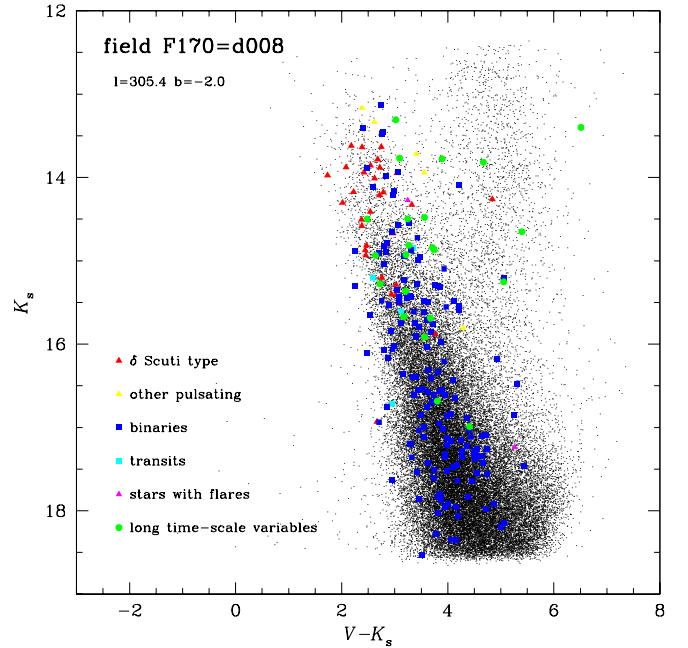


**Fig. 11.**  $J$  vs.  $J - K_s$  colour-magnitude diagrams for common VIMOS-VVV stars in the VIMOS fields F167 (left panel) and F170 (right panel). The solid lines roughly separate main-sequence from red giant stars.

elled CMD this area is populated by giants, subgiants, and luminous main-sequence stars ( $-0.5 < M_V < 2.0$  mag) of relatively high metallicities ( $-0.5 < [Fe/H] < 0.3$ ) located at distances  $10 < D < 18$  kpc. We tested models with different values of extinction and interstellar clouds beyond 10 kpc. The best result we achieved for the standard extinction  $a_V = 0.70$  mag/kpc and three



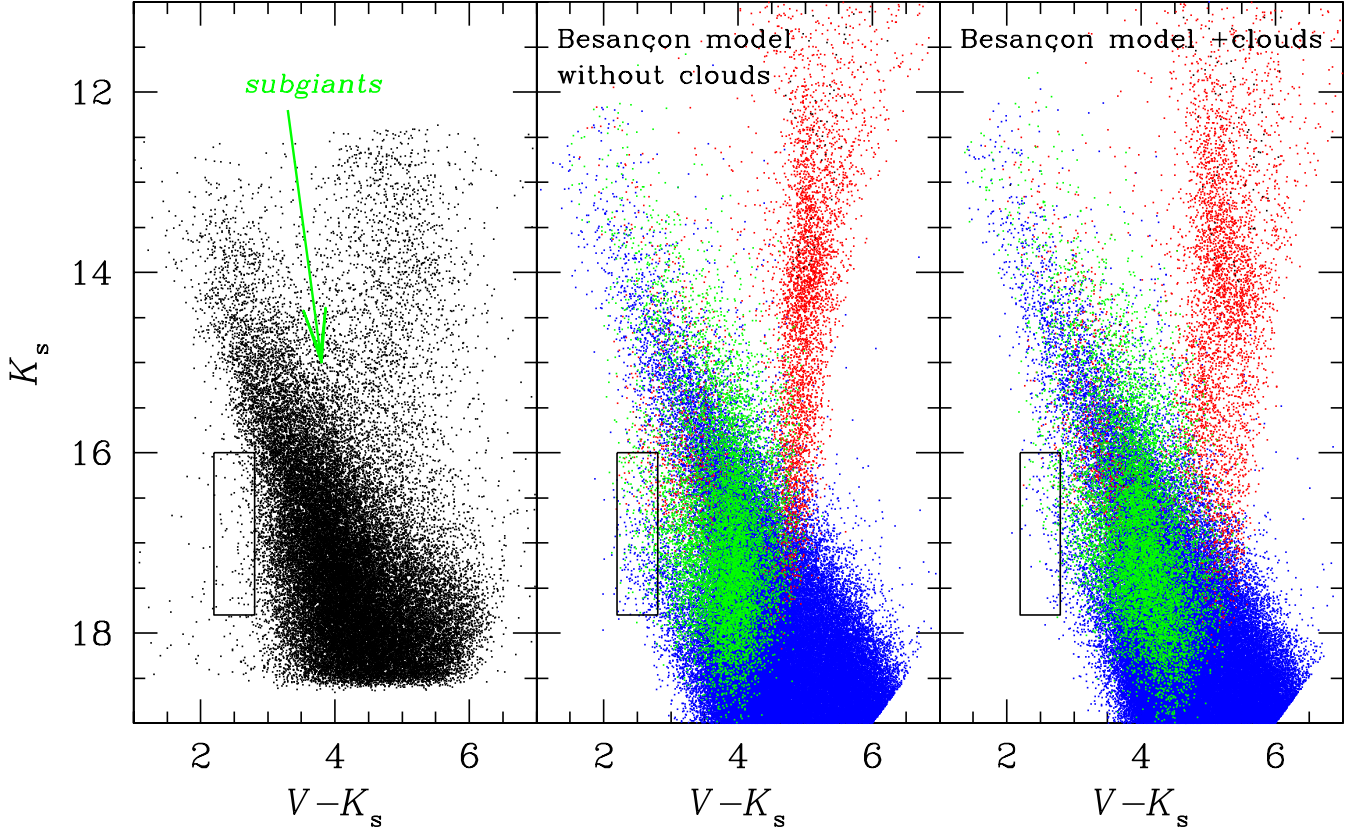
**Fig. 12.** Two ( $V - J$  vs.  $J - K_s$  and  $J - H$  vs.  $H - K_s$ ) colour-colour diagrams for common VIMOS-VVV stars in the VIMOS fields F167 and F170. Red giants selected in the CMDs in the previous figure are shown in red.



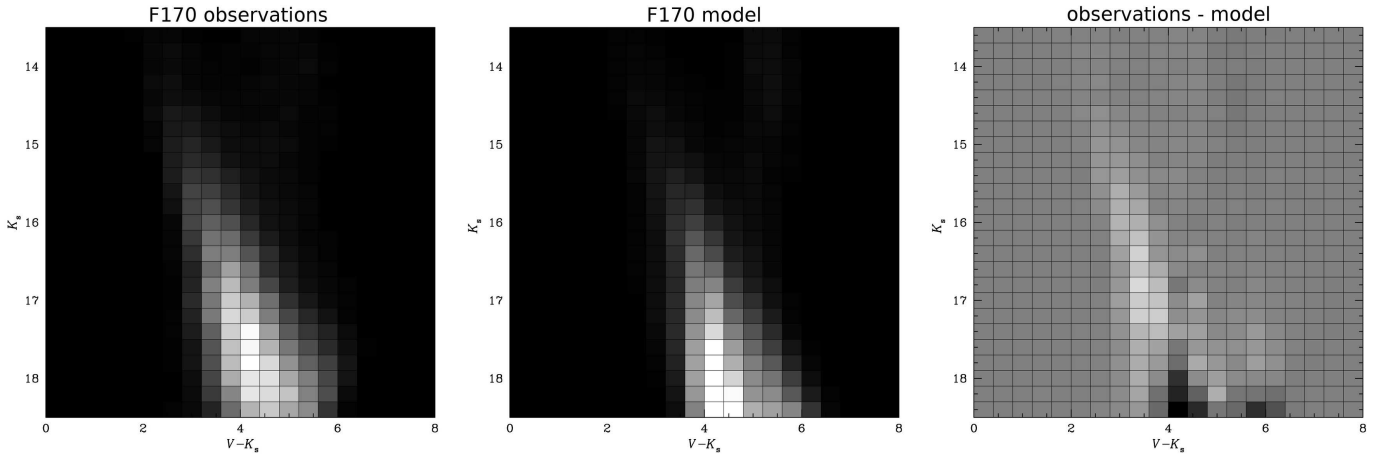
**Fig. 13.**  $K_s$  vs.  $V - K_s$  diagram with marked positions of 223 variables found in the VIMOS field F170.

absorbing clouds of  $a_V = 0.17$  mag each located at distances 11, 12, and 13 kpc from the Sun, respectively. These clouds would exist in the Carina-Sagittarius Arm, which is a minor Galactic arm located between the Scutum-Centaurus Arm and the distant extended spiral arm of the Milky Way (McClure-Griffiths et al. 2004). This model is presented in the right panel of Fig. 14. In

## field F170=d008



**Fig. 14.** Comparison of the observed (left panel) and two modelled  $K_s$  vs.  $V - K_s$  diagrams for the field F170. Stars of different luminosity classes are shown in colours: supergiants (class I) and bright giants (class II) in black, giants (class III) in red, subgiants (class IV) in green, main-sequence stars (class V) in blue. Both models are for the standard extinction  $a_V = 0.70$  mag/kpc, but the one in the right panel contains additional interstellar clouds at distances 11-13 kpc from the Sun. The wider spread in the  $V - K_s$  colour for giants and proper number of stars in the small box indicate that the model with the clouds provides the better fits.



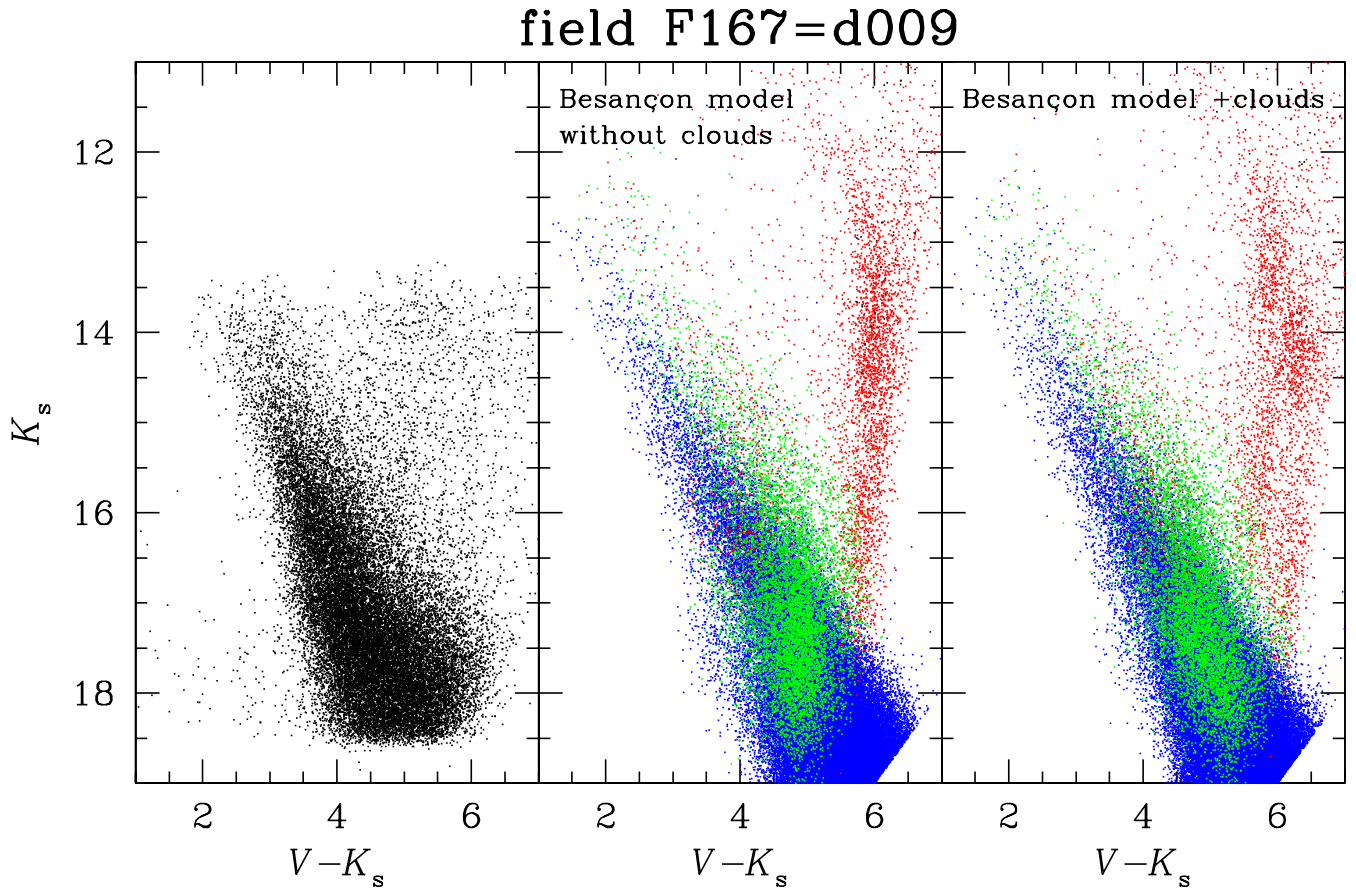
**Fig. 15.** Observed (left) and modelled (middle) Hess  $K_s$  vs.  $V - K_s$  CMDs. The subtraction of these two diagrams is shown in the right panel. For objects fainter than  $K_s \sim 17.5$  mag the data are incomplete.

Fig. 15 we show the result of subtraction of the observed and best-modelled CMDs.

Results of simulations for the field F167 are presented in Fig. 16. In this case we left the clouds, but we had to decrease the extinction to  $a_V = 0.68$  mag/kpc.

## 6. Conclusions

We have used deep optical data from VLT/VIMOS and near-IR data from VISTA to search for variable stars and to investigate stellar populations near the Galactic plane in the con-



**Fig. 16.** Comparison of the observed (left panel) and modelled  $K_s$  vs.  $V - K_s$  diagrams for field F167. The colours are the same as in Fig. 14. The model in the middle panel is for the standard extinction  $a_V = 0.70$  mag/kpc and does not contain absorbing clouds. The model in the right panel is for a lower extinction of 0.68 mag/kpc and contains clouds located at the same distances as in the best model for F170, i.e. at 11-13 kpc from the Sun.

stellation Centaurus. In the VIMOS field F170 in a series of 583  $V$ -band images spread over two nights we have detected 333 variables among 84 734 stars with brightness in the range  $12.7 < V < 26$  mag. Only four of these objects were previously known. For 263 variables we were able to assess the periods. Fifty-three of the newly discovered variables are pulsating stars, mostly of  $\delta$  Scuti type. Thirty-eight objects show brightness variations on long-time scales, and require a longer timeline of observations to derive their period and mean luminosity.

Among all observed variables 241 are classified as eclipsing/ellipsoidal binaries, which is 0.284% of the whole sample of searched stars. In Table 4 we compare this result with the rate of binaries detected in Galactic fields in other recent ground-based variability studies as well as in the *Kepler* space mission. The simple search method we applied to our short-period data, the eye inspection of all light curves, turned out to be very effective. It is interesting that we have obtained almost the same rate of eclipsing/ellipsoidal systems as in our previous search in a VIMOS field in Carina (Pietrukowicz et al. 2009). The binary detection rate would be very probably higher if the observations lasted considerably longer than only two days. Preliminary results from the *Kepler* space mission show that after the first 44 days of operation the average occurrence rate of binary systems is  $\sim 1.2\%$  (Prša et al. 2011). However, the *Kepler* photometry is much more accurate, which allows the detection of a larger part of lower amplitude variables than the other ground-based

surveys. About 51% of 1879 eclipsing/ellipsoidal binary stars detected by *Kepler* have orbital periods shorter than 1.44 days, whereas in the VIMOS sample 203 out of 241 binary systems have orbital periods  $< 1.44$  d. Assuming the same binary occurrence rate in all directions of the Milky Way we estimate that one can find up to  $\sim 0.5\%$  of binaries in ground-based data using an image subtraction technique.

In the second part of this work we have combined the  $V$ -band data from VIMOS with  $JHK_s$ -band photometry from VISTA. This has been done for the VIMOS fields F167 and F170. We presented optical-IR colour-magnitude and colour-colour diagrams. By subtracting CMDs for field F167 from field F170 we confirmed that the reddening in field F167, which is located slightly closer to the Galactic plane, is indeed higher than in F170. From the location of the detected variables in the CMD we conclude that probably all objects belong to main-sequence stars in the Scutum-Centaurus Arm.

From the comparison of the observed  $K_s$  vs.  $V - K_s$  diagrams with different synthetic diagrams based on the Galactic model of Besançon we conclude the presence of interstellar clouds at distances 11-13 kpc from the Sun. The clouds may belong to the minor Carina-Sagittarius Arm located between the Scutum-Centaurus Arm and the distant extended spiral arm of the Milky Way.

The results presented in this paper, including the large number of newly discovered variables in a relatively small field,

**Table 4.** Percentage of detected binaries in our search in comparison with other ground-based surveys and recent results from the *Kepler* space mission (the last row).

Authors	Field	Period of obs.	Method of searches	Total number of stars	Percentage of ecl/ell
Paczyński et al. (2006)	$\delta < +28^\circ$	5-8 years	Fourier	17,000,000	0.065 %
Weldrake & Bayliss (2008)	0.751 deg <sup>2</sup> , Lup	53 nights	AoV	110,372	0.172 %
Pietrukowicz et al. (2009)	0.052 deg <sup>2</sup> , Car	4 nights	by eye & AoV	50,897	0.291 %
Miller et al. (2010)	0.25 deg <sup>2</sup> , Nor	58 nights	LSA	335,592	0.301 %
This work	0.052 deg <sup>2</sup> , Cen	2 nights	by eye	84,734	0.284 %
Prša et al. (2011)	105 deg <sup>2</sup> , Cyg-Lyr	44 days	BLS	156,097	1.204 %

high-quality photometry, and the construction of deep optical-IR colour-magnitude diagrams demonstrate that ground-based wide-field multiple-band variability surveys are powerful tools for drawing a detailed picture of our Galaxy.

*Acknowledgements.* PP is supported by funding to the OGLE project from the European Research Council under the European Community's Seventh Framework Programme (FP7/2007-2013)/ERC grant agreement no. 246678, and by the grant No. IP2010 031570 financed by the Polish Ministry of Sciences and Higher Education under Iuventus Plus programme. This work is also supported by FONDAP Center for Astrophysics 15010003, BASAL Center for Astrophysics and Associated Technologies PFB-06, MILENIO Milky Way Millennium Nucleus P-07-021-F, FONDECYT 1090213 from CONICYT, and the European Southern Observatory.

## References

- Alard, C., & Lupton, J. 1998, *ApJ*, 503, 325
- Alcock, C., Allsman, R. A., Alves, D. R., et al. 1998, *ApJ*, 492, 190
- Alcock, C., Allsman, R. A., Alves, D. R., et al. 2000, *ApJ*, 542, 281
- Bakos, G., Noyes, R. W., Kovács, G., et al. 2004, *PASP*, 116, 266
- Churchwell, E., Babler, B. L., Meade, M. R., et al. 2009, *PASP*, 121, 213
- Díaz, R. F., Ramírez, S., Fernández, J. M., et al. 2007, *ApJ*, 660, 850
- Fernández, J. M., Minniti, D., Pietrzyński, G., et al. 2006, *ApJ*, 647, 587
- Hoyer, S., Ramírez Alegria, S., Ivanov, V. D., et al. 2007, *ApJ*, 669, 1345
- Ivezić, Ž., Tyson, J. A., Allsman, R., et al. 2008, arXiv:0805.2366
- Kaiser, N., et al. 2002, American Astronomical Society, 201st AAS Meeting, Bulletin of the AAS, 34, 1304
- Koch, D. G., Borucki, W. J., Basri, G., et al. 2010, *ApJ*, 713, L79
- LeFevre, O., Saisse, M., Mancini, D., et al. 2003, *SPIE*, 4841, 1670
- Lucas, P. W., Hoare, M. G., Longmore, A., et al. 2008, *MNRAS*, 391, 136
- McClure-Griffiths, N. M., Dickey, J. M., Gaensler, B. M., & Green, A. J. 2004, *ApJ*, 607, L127
- Miller, V. R., Albrow, M. D., Afonso, C., & Henning, Th. 2010, *A&A*, 519, A12
- Minniti, D., Fernández, J. M., Díaz, R. F., et al. 2007, *ApJ*, 660, 858
- Minniti, D., Lucas, P. W., Emerson, J. P., et al. 2010, *New A*, 15, 443
- Minniti, D., Saito, R. K., Alonso-García, J., et al. 2011, *ApJ*, 733, 43
- Nataf, D. M., Stanek, K. Z., & Bakos, G. Á. 2010, *Acta Astron.*, 60, 261
- Paczyński, B., Szczygieł, D. M., Pilecki, B., & Pojmański, G. 2006, *MNRAS*, 368, 1311
- Pietrukowicz, P., Minniti, D., Fernández, J. M., et al. 2009, *A&A*, 503, 651
- Pietrukowicz, P., Minniti, D., Díaz, R. F., et al. 2010, *A&A*, 509, A4
- Pojmański, G. 2001, *ASP Conference Series*, 246, 53
- Pojmański, G., Pilecki, B., Szczygieł, D. 2005, *Acta Astron.*, 55, 275
- Prša, A., Batalha, N., Slawson, R. W., et al. 2011, *AJ*, 141, 83
- Robin, A. C., Reylé, C., Derrière, & Picaud, S. 2003, *A&A*, 409, 523
- Schechter, P. L., Mateo, M., & Saha, A. 1993, *PASP*, 105, 1342
- Schlegel, D. J., Finkbeiner, D. P., Davis, M. 1998, *ApJ*, 500, 525
- Stetson, P. B. 1987, *PASP*, 99, 191
- Szczygieł, D. M., Pojmański, G., Pilecki, B. 2009, *Acta Astron.*, 59, 137
- Udalski, A., Pietrzyński, G., Szymański, M., et al. 2003, *Acta Astron.*, 53, 133
- Udalski, A., Szymański, M., Kubiak, M., et al. 2004, *Acta Astron.*, 54, 313
- Weldrake, D. T. F., & Bayliss, D. D. R. 2008, *AJ*, 135, 649
- Woźniak, P. R. 2000, *Acta Astron.*, 50, 421
- Woźniak, P. R., Udalski, A., Szymański, M., et al. 2002, *Acta Astron.*, 52, 129
- Woźniak, P. R. 2004, *AJ*, 127, 2436